Quantum dynamics of a particle with a spin-dependent velocity

2005 J. Phys. A: Math. Gen. 38 1

(http://iopscience.iop.org/0305-4470/38/1/001)

INSTITUTE OF PHYSICS PUBLISHING JOURNAL OF PHYSICS A: MATHEMATICAL AND GENERAL

J. Phys. A: Math. Gen. **38** (2005) 1–16 doi:10.1088/0305-4470/38/1/001

Quantum dynamics of a particle with a spin-dependent velocity

Claude Aslangul

Groupe de Physique des Solides, Laboratoire associé au CNRS (UMR 7588), Université Paris, Paris 6, Campus Boucicaut, 140 rue de Lourmel, 75015 Paris, France

E-mail: aslangul@gps.jussieu.fr

Received 8 June 2004, in final form 14 October 2004
Published 8 December 2004
Online at stacks.iop.org/JPhysA/38/1

Abstract

We study the dynamics of a particle in continuous time and space, the displacement of which is governed by an internal degree of freedom (spin). In one definite limit, the so-called quantum random walk is recovered but, although quite simple, the model possesses a rich variety of dynamics and goes far beyond this problem. Generally speaking, our framework can describe the motion of an electron in a magnetic sea near the Fermi level when linearization of the dispersion law is possible, coupled to a transverse magnetic field. Quite unexpected behaviours are obtained. In particular, we find that when the initial wave packet is fully localized in space, the J_z angular momentum component is frozen; this is an interesting example of an observable which, although it is not a constant of motion, has a constant expectation value. For a non-completely localized wave packet, the effect still occurs although less pronounced, and the spin keeps for ever memory of its initial state. Generally speaking, as time goes on, the spatial density profile looks rather complex, as a consequence of the competition between drift and precession, and displays various shapes according to the ratio between the Larmor period and the characteristic time of flight. The density profile gradually changes from a multimodal quickly moving distribution when the scattering rate is small, to a unimodal standing but flattening distribution in the opposite case.

PACS numbers: 03.67.Lx, 05.40.Fb, 72.10.Fk, 72.25.−b, 85.75.−d

1. Introduction

The term *quantum random walk* was coined some time ago by Aharonov and Davidovich [1] to qualify the motion of a quantum particle moving either left or right according to the value of the J_z component of its spin. As such, this is completely different from the quantum

Brownian motion problem, in which one fully describes in a quantum framework the motion of a single (light) particle moving in a bath of heavy particles—a quantum version of the classical Brownian motion. This latter problem has been the subject of many papers in the past, revivified in the 1980s by the pioneering work of Caldeira and Leggett (for a review, see Leggett *et al* [2]), showing that for the so-called ohmic coupling with the bath, dynamical symmetry breaking occurs above a given threshold. On a more elementary level, simple models show how the classical Brownian motion can be generalized to the quantum world, although long time scales (and algebraic behaviours) appear in correlation functions at small enough temperature, as shown by Aslangul *et al* [3]. We shall adopt here the recent meaning as proposed by Aharonov and Davidovich, shortened to QRW in the following.

This latter problem is presently the subject of intense activity, following the basic papers by Ambainis *et al* [4], Nayak and Vishwanath [5], Dür *et al* [6] and Konno [7] (for a recent comprehensive review, see the preprint by Kempe [8]). The basic motivation lies in the fact that QRW yields a dynamics at the opposite of classical random walk: for a spin $1/2$ particle, and a symmetric initial spin state with definite phases (see below for details), the probability density in space $P_{\mathrm{QRW}}(x,t)$ displays two well-defined peaks, moving away linearly in time from the starting place. This is to be contrasted with the $t^{1/2}$ spreading of the classical packet, the particle staying (in the average) at its starting point when no drift is present. It can be said that QRW, except for oscillations in spatial density, displays the same basic features as the classical non-diffusive motion with a drift (which can be obtained from the *biased* diffusion equation $\frac{\partial P}{\partial t} = -\vec{\nabla}[\vec{v}P - D\vec{\nabla}P]$—in the (singular) limit $D \to 0$, as explained for instance in the book by Gardiner [9]), when the velocity itself is a random variable assuming two values $\pm v_0$ with definite probabilities. This rather intuitive picture has been firmly grounded by the recent work of Blanchard and Hongler [10].

Due to the quantum nature of the walk, all steps are strongly correlated (as contrasted to classical motion), as it is also the case for repeated measurements yielding the Zeno paradox theoretically found by Misra and Sudarshan [11] and observed by Itano *et al* [12]; this means that specific ever-lasting correlations are always relevant. One consequence is that the linear dimension of the visited space increases linearly in time, i.e. much more rapidly for QRW than for classical motion. It is hoped, on a somewhat speculative level, that Monte Carlo algorithms could be improved by drawing benefit of this fact (see, e.g., Kempe [13]).

We adopt here a more general point of view. Indeed, we define a simple model containing a single parameter, denoted α in the following, which is essentially the product of the spin-flip rate by the time of flight in space. As shown below, the limit $\alpha \to 0$ can be viewed as the continuous space–time version of the conventional QRW. Out of this limiting case, the model can describe the dynamics of an electron near the Fermi level (once the dispersion law has been linearized, $\varepsilon(k) \to \pm\hbar(k - k_{\mathrm{F}})v_{\mathrm{F}}$ as is done e.g. in the Luttinger model [14]), moving in a magnetic sea created by impurities, or coupled to nuclear spins (Vagner [15]). Elastic collisions with the magnetic background can flip the spin of the moving electron and, simultaneously, change its velocity from $+v_{\mathrm{F}}$ to $-v_{\mathrm{F}}$. Alternatively, such a reversal can be induced by a transverse magnetic field forcing the spin to precess harmonically at the Larmor frequency ω. As a whole, spin and orbital degrees of freedom are coupled, yielding intrication of the state as time goes on, and competition between precession and translation in space. This produces interesting effects; the first one (and probably the most unexpected) is freezing of the precession when the initial packet is quite narrow—an effect which could have interesting applications in spintronics, as well in two-dimensional systems (McGuire *et al* [16]), in carbon nanotubes (Yang *et al* [17]), in quantum dots (Levitov and Rashba [18]) and in semiconductors (Dyakonov [19]). A second characteristic feature is the $\propto t$ spreading of the wavepacket which arises in any case, even when the precession is extremely rapid: because of the latter, the

particle has no time to choose between right and left moves, but dispersion still occurs, and very quickly as compared to classical random motion.

Obviously, the physical relevance of our model is subjected to small deviations around k_F. On the other hand, it is hoped that the basic (and surprising) results found below retain some relevance even with such restrictions, and at least can take place on space and time scales to be specified in real life. It is worthy to note that, provided such a physical picture is meaningful, α becomes an easily tunable parameter by varying either the magnetic field, or the filling ratio of the band, or the density of the magnetic diffusing centres.

This paper is organized as follows. We first define the model (section 2), explicitly show the relation between our model and QRW, and give a qualitative discussion of limiting cases. We then briefly derive the equations giving the time evolution of the density for an arbitrary spin J (section 3), on which the spin locking due to space confinement in the $\alpha \to 0$ limit can be directly shown. This fact is confirmed by a detailed study of the average value J_z section 4). Then, we focus on the $J = \frac{1}{2}$ case (section 5), and calculate the density profile $P(x, t)$, which displays many various shapes, some unexpected when the two time scales related to the Larmor precession and the displacement in space are of the same order of magnitude. Eventually, conclusions are drawn and hints for future work are given. In the appendix, details are given on the asymptotic analytical work required to get insight on the features of the probability density.

2. Model and qualitative discussion

For a spin $\vec{J}$ particle, our model Hamiltonian reads

$$H = \omega J_y + \hbar^{-1} \vec{v} \cdot \hat{\vec{p}} J_z. \tag{2.1}$$

In this expression, ω is the spin-flip rate due to scattering on impurities, or the Larmor frequency due to a transverse magnetic field along the y direction. $\vec{v}$ is the (scalar) quantity defining the velocity scale, $\hat{\vec{p}}$ is the momentum ($\hat{p} = -\mathrm{i}\hbar\vec{\nabla}$ in the q-representation). Despite some similarity at first glance, the Hamiltonian (2.1) has nothing to do with the Dirac Hamiltonian, in which the momentum is coupled to the Dirac $\vec{\alpha}$ matrices; indeed, the angular momentum (spin) is not given there by $\vec{\alpha}$ and, in addition, the problem has here the dimensionality $2J + 1$ in spin space, instead of four in the Dirac theory. Also note that, in its one-dimensional form, with a space-dependent ω and for $J = 1/2$, this Hamiltonian has been used in various contexts such as inhomogeneous superconductors (de Gennes [20]) and solitons in polyacetylene (Takayama *et al* [21]).

In the following, we restrict ourselves to one-dimensional space; calling Ox the line on which the particle moves, the Hamiltonian (2.1) simplifies to

$$H = \omega J_y + \hbar^{-1} v \hat{p} J_z, \qquad \hat{p} = -\mathrm{i}\hbar \frac{\partial}{\partial x}. \tag{2.2}$$

Note that the label x of direction of motion and the three directions defining the components J_x, J_y and J_z generally have no relations between them. Also note that the 'kinetic' term is invariant under time reversal.

2.1. Continuous limit of the quantum Brownian walk

In order to perform the continuous limit of QRW, let us recall the basic formalism. In the original model [6], the spin-$\frac{1}{2}$ particle hops on a one-dimensional infinite lattice (lattice spacing a, $n \in \mathbf{Z}$) from one site to the two first-neighbours, either right or left according to the

value + or − of the J_z component. In obvious notations, the operator S generating this spatial motion is

$$S = |+\rangle\langle +| \otimes \sum_n |n+1\rangle\langle n| + |-\rangle\langle -| \otimes \sum_n |n-1\rangle\langle n|. \tag{2.3}$$

Once a jump is done, the spin is changed by the action of a Hadamard matrix T acting on the $|\pm\rangle$ spin states, which we choose of the following form:

$$T = \frac{1}{\sqrt{2}} \begin{bmatrix} 1 & -1 \\ 1 & 1 \end{bmatrix}. \tag{2.4}$$

Thus, one step of the motion is generated by the product TS, which reflects the basic sequential nature of the walk. As a whole, for integer times t, the state $|\Psi(t)\rangle$ obeys the following equation:

$$|\Psi(t+1)\rangle = TS|\Psi(t)\rangle \equiv H_{\mathrm{QRW}}|\Psi(t)\rangle. \tag{2.5}$$

Performing now a Fourier transformation in space $\left(|k\rangle = N^{-1/2}\sum_n \mathrm{e}^{\mathrm{i}kna}|n\rangle\right)$, one obtains

$$H_{\mathrm{QRW}} = \sum_k \mathrm{e}^{-\mathrm{i}\hbar^{-1}\frac{\pi}{2}J_y}\,\mathrm{e}^{-\mathrm{i}\hbar^{-1}kaJ_z}|k\rangle\langle k|. \tag{2.6}$$

Let us now formally replace $t+1$ by $t+\Delta t$, $\frac{\pi}{2}$ by $\omega\Delta t$ in the first exponential; taking the limit $a \to 0$, $\Delta t \to 0$, $\frac{a}{\Delta t} = \mathrm{Const} \equiv v$, one has

$$H_{\mathrm{QRW}} \to \mathbf{1} + \frac{\Delta t}{\mathrm{i}\hbar}\sum_k (\omega J_y + kvJ_z)|k\rangle\langle k|. \tag{2.7}$$

Going back to direct space, and taking now the limit $\lim_{\Delta t\to 0}\frac{1}{\Delta t}[|\Psi(x,t+\Delta t)\rangle - |\Psi(x,t)\rangle]$, (2.5) yields

$$\mathrm{i}\hbar\frac{\partial}{\partial t}|\Psi(x,t)\rangle = H|\Psi(x,t)\rangle \tag{2.8}$$

where H is the Hamiltonian given in (2.2). This Schrödinger equation retains the two essential features of QRW: the direction of the motion is determined by the value of the J_z component, and the latter is not a constant of motion due to the transverse magnetic field (external or intrinsic) to which the particle is coupled though the operator J_y.

Yet, a basic difference exists between H_{QRW} and H, due to the fact that in the discrete version, the particle jumps, and *then* the spin is changed by T: as already mentioned, the rules of the game are essentially sequential, allowing us to state that the spin changes slowly as compared to the time of flight. In contrast, with H given in (2.2), both motion and spin-flip occur simultaneously. This means that, within the framework defined by H, one expects to recover the quantum random motion only when the Larmor frequency ω is quite small as compared to the time scale of the displacement. As it stands, the Hamiltonian H thus defines a model for which ordinary QRW is just one limit.

One additional ingredient is required, namely the initial state, which will be chosen of the spin-space separate form:

$$|\Psi(x,t=0)\rangle = \psi(x)\otimes\sum_{M=-J}^{+J} c_M|M\rangle \equiv \psi(x)\otimes|\chi\rangle. \tag{2.9}$$

$|M\rangle$ is the eigenstate of J_z with the eigenvalue $M\hbar$; for physical purpose, $\psi(x)$ is chosen as a localized even function with a width σ, assuming real values in order to avoid any built-in inessential drift; for explicit calculations, we retain the Gaussian normalized form:

$$\psi(x) = (\sqrt{2\pi}\sigma)^{-1/2}\,\mathrm{e}^{-x^2/(4\sigma^2)}. \tag{2.10}$$

Obviously, the state becomes intricate as time goes on, and one generally has at time $t > 0$:

$$|\Psi(x,t)\rangle = \sum_{M=-J}^{+J} \psi_M(x,t)|M\rangle. \tag{2.11}$$

The main goal is to find the probability density in space, given by

$$P(x,t) = \sum_{M=-J}^{+J} |\psi_M(x,t)|^2. \tag{2.12}$$

The model is now completely defined, and involves just one dimensionless parameter, called α in all the following:

$$\alpha = \frac{\sigma\omega}{v}. \tag{2.13}$$

When α is large, the spin undergoes many Larmor precessions during a relatively small displacement in space; in contrast, α small means that the spin precesses quite slowly when moving in space.

2.2. The limiting cases

Let us now briefly describe the limiting cases. As explained above, the $\alpha \to 0$ limit must reproduce QRW. More precisely, when the Larmor period becomes much larger than any other relevant time scale, the limit of the spatial density is the $(2J+1)$-modal distribution:

$$\lim_{\alpha\to 0} P(x,t) = \sum_{M=-J}^{+J} |c_M|^2 |\psi(x - Mvt)|^2 \qquad \forall t \tag{2.14}$$

(for $J = 1/2$, the two-peak splitting of ordinary QRW is recovered). Such a density trivially gives $\langle x\rangle(t) = vt\sum_M \hbar^{-1}\langle J_z\rangle(0)$ and $\Delta x^2(t) = (vt)^2\hbar^{-2}\Delta J_z^2(0)$. The $\propto t^2$ increase of its mean-square deviation merely reflects the fact that each peak of the density moves away linearly in time due to the persisting multimodal character of the density profile, which is frankly different from *spreading* in the usual sense. Note that, in the limit $\alpha = 0$, the relative phases of the c_M play no role, a symmetry which is broken for any finite α: in the general case, these phases are essential (see below) and, in particular, determine whether the density $P(x,t)$ is symmetric in space or not.

On the other hand, when α goes to infinity, spin and space degrees of freedom become decoupled. Thus the spin stays immobile, and simply precesses within its initial wave packet, which remains as it stood at the beginning:

$$\lim_{\alpha\to+\infty} P(x,t) = |\psi(x)|^2 \qquad \forall t. \tag{2.15}$$

It will be seen in the following that these two trivial limits are indeed singular, especially the limit $\alpha \to 0$ (because the velocity v is in factor of the highest derivative in H); this can be considered as a first symptom of the richness of the dynamics for any *finite* α. Anyway, the above limiting behaviours of $P(x,t)$ are expected to hold approximately true in the general case for times $t \ll \frac{2\pi}{\omega}$ and $t \ll \frac{\sigma}{v}$, respectively and mimic the actual dynamics.

3. Formal expression of the density

The Schrödinger equation (2.8) is formally easily solved by going to the p-representation. It then reads

$$\mathrm{i}\hbar\frac{\partial}{\partial t}|\Phi(p,t)\rangle = (\omega J_y + \hbar^{-1}vpJ_z)|\Phi(p,t)\rangle, \tag{3.1}$$

where $|\Phi(p,t)\rangle$ is the p-representation of the state at time t (p is now a scalar). The time-evolution operator $U(p,t)$ is such that

$$|\Phi(p,t)\rangle = U(p,t)|\Phi(p,0)\rangle, \tag{3.2}$$

where $|\Phi(p,0)\rangle \equiv \phi(p)\otimes|\chi\rangle$ is the p-representation of the initial state (2.9); with the Gaussian (2.10), one has

$$\phi(p) = \left(\frac{2\sigma}{\hbar\sqrt{2\pi}}\right)^{\frac{1}{2}} \mathrm{e}^{-\sigma^2 p^2/\hbar^2}. \tag{3.3}$$

By introducing the p-dependent unitary transformation $R(p) = \mathrm{e}^{(\mathrm{i}\hbar)^{-1}\theta(p)J_x}$, $U(p,t)$ assumes the form

$$U(p,t) = R^\dagger(p)\,\mathrm{e}^{-\mathrm{i}\hbar^{-1}\Omega(p)tJ_z}R(p), \tag{3.4}$$

where

$$\Omega(p) = [\omega^2 + (v\hbar^{-1}p)^2]^{\frac{1}{2}}, \tag{3.5}$$

$$\cos\theta(p) = \frac{v\hbar^{-1}p}{\Omega(p)}, \qquad \sin\theta(p) = \frac{\omega}{\Omega(p)}. \tag{3.6}$$

This allows us to write down the formal expression of the Fourier transform of the density probability, $\mathcal{P}(k,t) = \int_{-\infty}^{+\infty}\mathrm{d}x\,\mathrm{e}^{\mathrm{i}kx}P(x,t)$, as the following:

$$\mathcal{P}(k,t) = \int_{-\infty}^{+\infty}\mathrm{d}p\,\phi_+^*\phi_-\langle\chi|U^\dagger\left(p+\frac{\hbar k}{2},t\right)U\left(p-\frac{\hbar k}{2},t\right)|\chi\rangle, \tag{3.7}$$

where $\phi_\pm = \phi(p\pm\hbar k/2)$. For arbitrary J, such an expression seems untractable as it stands, but it allows us to look at the limiting case $\alpha\to 0$, which can be obtained by assuming a fully localized packet ($\sigma = 0+$). Starting with the initial Gaussian wavepacket (2.10), a careful limiting procedure yields

$$\lim_{\alpha\to 0}\mathcal{P}(k,t) = \sqrt{\frac{2}{\pi}}\int_{-\infty}^{+\infty}\mathrm{d}\xi\,\mathrm{e}^{-2\xi^2}\langle\chi|\mathrm{e}^{\mathrm{i}kvt\hbar^{-1}J_z}|\chi\rangle. \tag{3.8}$$

From this, one immediately obtains the limiting expression of the probability density in direct space:

$$\lim_{\alpha\to 0}P(x,t) = \sum_{M=-J}^{+J}|c_M|^2\delta(x-Mvt). \tag{3.9}$$

This says that the initial narrow packet splits off in $2J+1$ components, each of them going away from the starting point with its own velocity Mv. Expression (3.9) holds true for any J and any initial spin state.

This result is at first surprising (it would also trivially occur in the absence of magnetic background or of the transverse field ($\omega = 0$)—which also gives $\alpha = 0$). It means that extreme confinement ($\sigma = 0$) of the spin forces the component J_z to have a constant expectation value, although J_z is not a constant of motion due to the fact that $\omega \neq 0$. Obviously enough, one can question the validity of the above limiting procedure, because the value $\alpha = 0$ is indeed singular; in fact, the above result, which provides an oversimplified picture of the spin-freezing phenomenon, can be easily confirmed by analysing an innocent-looking observable (indeed J_z itself), directly obtained by the Heisenberg equations. This is done in the following section for arbitrary α.

4. Dynamics of the coordinate and of the component J_z

In order to get more insight into the above result, we now solve the Heisenberg equations of motion. We write

$$\dot{x}_{\rm H} = v\hbar^{-1}J_{z{\rm H}}, \qquad \dot{p}_{\rm H} = 0, \qquad \dot{J}_{z{\rm H}} = -\omega J_{x{\rm H}}. \tag{4.1}$$

$$\dot{J}_{x{\rm H}} = \omega J_{z{\rm H}} - \hbar^{-1}vp_{\rm H}J_{y{\rm H}}, \qquad \dot{J}_{y{\rm H}} = \hbar^{-1}vp_{\rm H}J_{x{\rm H}}. \tag{4.2}$$

These equations can be readily integrated to yield

$$J_{z{\rm H}}(t) = \vec{e}(t)\cdot\vec{J}, \tag{4.3}$$

$$x_{\rm H}(t) = x + v\hbar^{-1}\vec{T}(t)\cdot\vec{J}, \tag{4.4}$$

where $\vec{J}$ (resp. x) coincides with $\vec{J}_{\rm H}(0)$ (resp. $x_{\rm H}(0)$ and where the components of the scalar vectors $\vec{e}(t)$ and $\vec{T}(t)$ are

$$\begin{aligned} e_x(t) &= -\sin\theta\sin\Omega t, \\ e_y(t) &= \sin\theta\cos\theta(1-\cos\Omega t), \qquad (4.5)\\ e_z(t) &= \cos^2\theta + \sin^2\theta\cos\Omega t, \qquad (4.6) \end{aligned}$$

and $T_u(t) = \int_0^t e_u(t')\,{\rm d}t'$. The mean-square deviation of the coordinate is

$$\Delta x^2(t) = \Delta x^2(0) + (v\hbar^{-1})^2\sum_{u,v}(\langle T_uT_vJ_uJ_v\rangle - \langle T_uJ_u\rangle\langle T_vJ_v\rangle), \tag{4.7}$$

where the brackets denote averages over the initial state (see (2.9) and (3.3))—remember that Ω and θ are functions of p, see (3.5) and (3.6), and enter in a convolution with the Fourier transform of (2.10). For any separate initial state, the averages factorize: $\langle T_uJ_v\rangle = \langle T_u\rangle\langle J_v\rangle$ and so on.

These results allow a straightforward discussion displaying the strange features of the dynamics, especially the rather counterintuitive role of the initial spin state on the subsequent motion, especially on the symmetry of the probability density, as already discussed (see, e.g., the analysis by Kempe [8]).

Close inspection first shows the essential role of the phases of the coefficients c_M appearing in expansion (2.9). Indeed, it is readily seen that when the initial spin state is an eigenvector of J_y, then $\langle J_z\rangle(t)$ and $\langle x\rangle(t)$ are constant (and thus vanish at any time), whereas Δx^2 is still $\propto t^2$. Another consequence is that the density probability $P(x,t)$ is symmetric in space in this case, and only in this case. Thus, the dynamics, and the parity of the spatial density, strongly depend on the relative phases of the coefficients c_M defining the initial spin state (see (2.9)), not only of the weights $|c_M|^2$—a feature which clearly separates the general α-finite case from the $\alpha = 0+$ limit. For any other preparation, $P(-x,t) \neq P(x,t)$ and the expectation values $\langle J_z\rangle(t)$ and $\langle x\rangle(t)$ do vary in time, as exemplified below for a definite preparation.

Indeed, let us assume that the initial spin state is the eigenstate $|M\rangle$ of J_z ($J_z|M\rangle = M\hbar|M\rangle$); then, the expectation values at time t are

$$\langle J_z\rangle(t) = M\hbar\langle\cos^2\theta + \sin^2\theta\cos\Omega t\rangle, \tag{4.8}$$

$$\langle x\rangle(t) = Mvt\left\langle\cos^2\theta + \sin^2\theta\frac{\sin\Omega t}{\Omega t}\right\rangle, \tag{4.9}$$

$$\Delta x^2(t) = \sigma^2 + v^2\left[\frac{1}{2}[J(J+1) - M^2]\left\langle T_x^2 + T_y^2\right\rangle + M^2\left(\left\langle T_z^2\right\rangle - \langle T_z\rangle^2\right)\right]. \tag{4.10}$$

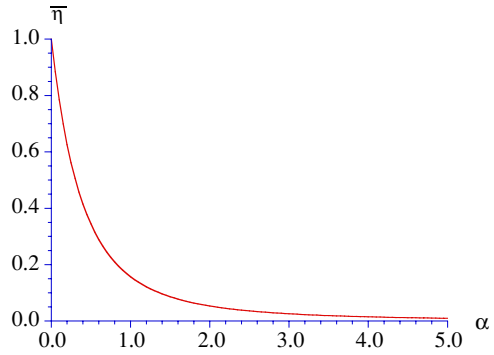

Figure 1. Variation of the time average $\overline{\eta}$ (see (4.13)) as a function of α.

In the preceding equations, $\langle\bullet\rangle$ denotes the average over the orbital variable:

$$\langle\bullet\rangle = \sqrt{\frac{2}{\pi}}\frac{\sigma}{\hbar}\int_{-\infty}^{+\infty}(\bullet)\,\mathrm{e}^{-2(\sigma p)^2/\hbar^2}\,\mathrm{d}p. \tag{4.11}$$

In particular, the expectation value of J_z is given by $\langle J_z\rangle(t) = \eta(t)\langle J_z\rangle(0)$ with

$$\eta(t) = \sqrt{\frac{2}{\pi}}\int_{-\infty}^{+\infty}\frac{\mathrm{e}^{-2\xi^2}}{\alpha^2+\xi^2}\left(\xi^2+\alpha^2\cos\sqrt{\alpha^2+\xi^2}\frac{\omega t}{\alpha}\right)\mathrm{d}\xi \tag{4.12}$$

(note that, with our definitions, $\frac{\omega t}{\alpha} = \frac{vt}{\sigma}$). $\eta(t)$ (obviously bounded by ±1) is clearly an oscillating function of time. This expression allows us to discuss the unexpected behaviour of the average value of J_z when α varies. First, let us look at the time-average value of η, $\overline{\eta} \equiv \lim_{t\to+\infty}\frac{1}{t}\int_0^t\eta(t')\,\mathrm{d}t'$. One readily finds

$$\overline{\eta} = 1 - \sqrt{2\pi}\alpha\,\mathrm{e}^{2\alpha^2}[1-\Phi(\sqrt{2}\alpha)] \tag{4.13}$$

where Φ is the probability integral [22]. $\overline{\eta}$ has the following behaviours:

$$\overline{\eta} \simeq \begin{cases} 1-\sqrt{2\pi}\alpha & \alpha \ll 1 \\ \dfrac{1}{4\alpha^2} & \alpha \gg 1. \end{cases} \tag{4.14}$$

In addition, it is readily seen that $1 - 2\overline{\eta} \leqslant \eta(t) \leqslant 1$. Thus, for α small, $\eta(t)$ oscillates around a value which is quite close to one, showing that $\langle J_z\rangle$ becomes nearly constant in time. In contrast, for α large, the oscillation takes place symmetrically around a quite small value. The variation of $\overline{\eta}$ as a function of α is given in figure 1.

At short times, one has $\eta(t) \simeq 1 - \frac{1}{2}(\omega t)^2$. The behaviour of $\eta(t)$ at large times is easily found by using a saddle-point method. We find

$$\eta(t) \simeq \overline{\eta} + \frac{2\alpha}{\sqrt{\omega t}}\cos\left(\omega t + \frac{\pi}{4}\right), \qquad t \gg \min\left(\frac{\sigma}{v}, \omega^{-1}\right). \tag{4.15}$$

The envelope of the oscillation around the time averaged value $\overline{\eta}$ thus decreases as $t^{-1/2}$. The variation of $\eta(t)$ at any time is plotted in figure 2 for two values of α.

These results confirm the confinement locking of the spin: whereas J_z is not a constant of motion, narrowing the width of the initial wave packet yields an expectation value which is less and less varying in time.

From (4.9), the average position of the particle is easily calculated and can be written as

$$\langle x\rangle(t) = Mvt\left[\overline{\eta} + \frac{\alpha^3}{\omega t}\sqrt{\frac{2}{\pi}}\int_{-\infty}^{+\infty}\frac{\mathrm{e}^{-2\xi^2}}{(\alpha^2+\xi^2)^{3/2}}\sin\sqrt{\alpha^2+\xi^2}\frac{\omega t}{\alpha}\,\mathrm{d}\xi\right]. \tag{4.16}$$

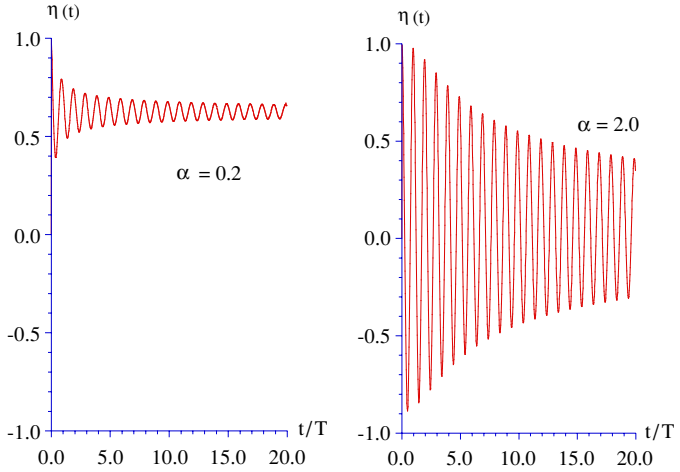

Figure 2. Variation in time of $\eta(t)$ for a narrow initial wave packet (left) and for a large one (right). For an infinitely narrow wave packet, $\langle J_z \rangle$ remains constant. The unit of time is one period T of the Larmor precession.

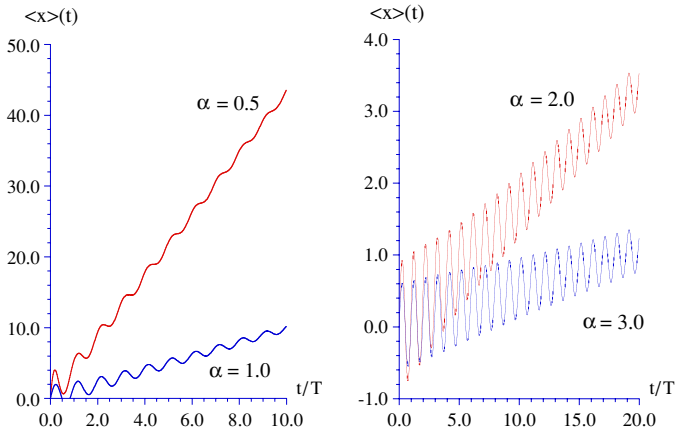

Figure 3. Variation in time of $\langle x \rangle(t)$ for four values of α, when the initial state is an eigenvector of J_z. Note the different horizontal and vertical scales.

This represents a drift motion, with a damped-in-time ($\propto t^{-1}$) oscillation around the central position $Mvt\overline{\eta}$, imaging the forward/backward motion of the particle within its wavepacket as the spin precesses, causing inversion of the velocity.

It is readily seen that $\langle x \rangle(t)$ is bounded for any time and any α; one finds

$$Mvt[\overline{\eta} - (\omega t)^{-1}] < \langle x \rangle(t) < Mvt[\overline{\eta} + (\omega t)^{-1}]. \tag{4.17}$$

This shows that, for such a preparation, the motion is always ballistic and simply approaches $\langle x \rangle(t) \simeq M\overline{\eta}vt$ at times which are large compared to the precession time scale. However, note that the effective velocity $\overline{\eta}v$ decreases rapidly when α becomes large (see (4.14) and figure 3). In the asymptotic regime, one precisely has

$$\langle x \rangle(t) \simeq Mvt\left[\overline{\eta} + \frac{2\alpha}{(\omega t)^{3/2}} \sin\left(\omega t + \frac{\pi}{4}\right)\right]. \tag{4.18}$$

Note that in the limit $\alpha \to 0$ but for an arbitrary initial spin state, one has $\langle J_z\rangle(t) = \langle J_z\rangle(0)$ and

$$\langle x\rangle(t) = vt\hbar^{-1}\langle J_z\rangle(0), \qquad \Delta x^2(t) = v^2t^2\hbar^{-2}\Delta J_z^2(0), \tag{4.19}$$

in agreement with (3.9). The $\propto t^2$ increase of the mean-square dispersion merely reflects the fact that in this limit, the density is just the superposition of the $2J + 1$ Dirac functions $\delta(x - Mvt)$.

Obviously, the mean-square deviation gives a first impression about the spatial density, but the qualitative discussion given above convinces one that a given t^2 increase of $\Delta x^2(t)$ can be realized in a variety of ways, ranging from two moving sharp peaks to a Gaussian-like flattening *in situ*. Clearly, a more precise analysis of the profile is required, and this is done in the following section for the $J = 1/2$ case.

5. Time evolution of the spatial density in the spin $\frac{1}{2}$ case

In the $J = 1/2$ case, the evolution operator can be easily written explicitly. After some algebra, we find the propagator $U(p, t)$ as the following:

$$U(p,t) = \cos\frac{\Omega(p)t}{2}\mathbf{1} - \mathrm{i}\sin\frac{\Omega(p)t}{2}\cos\theta(p)\sigma_z - \mathrm{i}\sin\frac{\Omega(p)t}{2}\sin\theta(p)\sigma_y \tag{5.1}$$

where the σ_u are the Pauli matrices. From this, one readily obtains the amplitudes $\psi_\pm(x, t)$, given by

$$\psi_\pm(x,t) = \frac{1}{\sqrt{2\pi\hbar}}\int_{-\infty}^{+\infty}\mathrm{d}p\,\mathrm{e}^{\frac{\mathrm{i}}{\hbar}px}\left[\left(\cos\frac{\Omega(p)t}{2} \mp \mathrm{i}\cos\theta(p)\sin\frac{\Omega(p)t}{2}\right)c_\pm \right.$$
$$\left. \mp \sin\theta(p)\sin\frac{\Omega(p)t}{2}c_\mp\right]\phi(p). \tag{5.2}$$

Close inspection of the integrals in (5.2) again reveals that for any initial state which is even and real, the density $P(x, t) = \sum_{\varepsilon=\pm}|\psi_\varepsilon(x, t)|^2$ is even only when $|c_+|^2 = |c_-|^2$ *and* $\frac{c_+}{c_-}$ purely imaginary, i.e. when the initial spin state is an eigenvector of J_y. In all other cases, $P(-x, t) \neq P(x, t)$.

In the following, we restrict to the symmetric case, taking $c_+ = \frac{1}{\sqrt{2}}$ and $c_- = \frac{\mathrm{i}}{\sqrt{2}}$, corresponding to $|\chi\rangle = |+\rangle_y$. Then, the density can be written as follows:

$$P(x,t) = \frac{1}{\sqrt{2\pi}\sigma}\sum_{r=1,2,3}|I_r(x,t)|^2, \tag{5.3}$$

where the three quantities I_r are given integrals. With the Gaussian wave packet (3.3), the latter explicitly write $\left(X = \frac{x}{\sigma}\right)$

$$I_1(x,t) = \frac{\alpha}{\sqrt{\pi}}\int_{-\infty}^{+\infty}\mathrm{d}\xi\,\frac{\mathrm{e}^{-\xi^2+\mathrm{i}\xi X}}{\sqrt{\alpha^2+\xi^2}}\sin\sqrt{\alpha^2+\xi^2}\,\frac{vt}{2\sigma}, \tag{5.4}$$

$$I_2(x,t) = \frac{1}{\sqrt{\pi}}\int_{-\infty}^{+\infty}\mathrm{d}\xi\,\mathrm{e}^{-\xi^2+\mathrm{i}\xi X}\,\frac{\xi}{\sqrt{\alpha^2+\xi^2}}\sin\sqrt{\alpha^2+\xi^2}\,\frac{vt}{2\sigma}, \tag{5.5}$$

$$I_3(x,t) = \frac{1}{\sqrt{\pi}}\int_{-\infty}^{+\infty}\mathrm{d}\xi\,\mathrm{e}^{-\xi^2+\mathrm{i}\xi X}\cos\sqrt{\alpha^2+\xi^2}\,\frac{vt}{2\sigma}. \tag{5.6}$$

These expressions allow an easy numerical calculation of the density $P(x, t)$ in various cases; the results are shown in figure 4 and display the extreme variety of $P(x, t)$ when the single

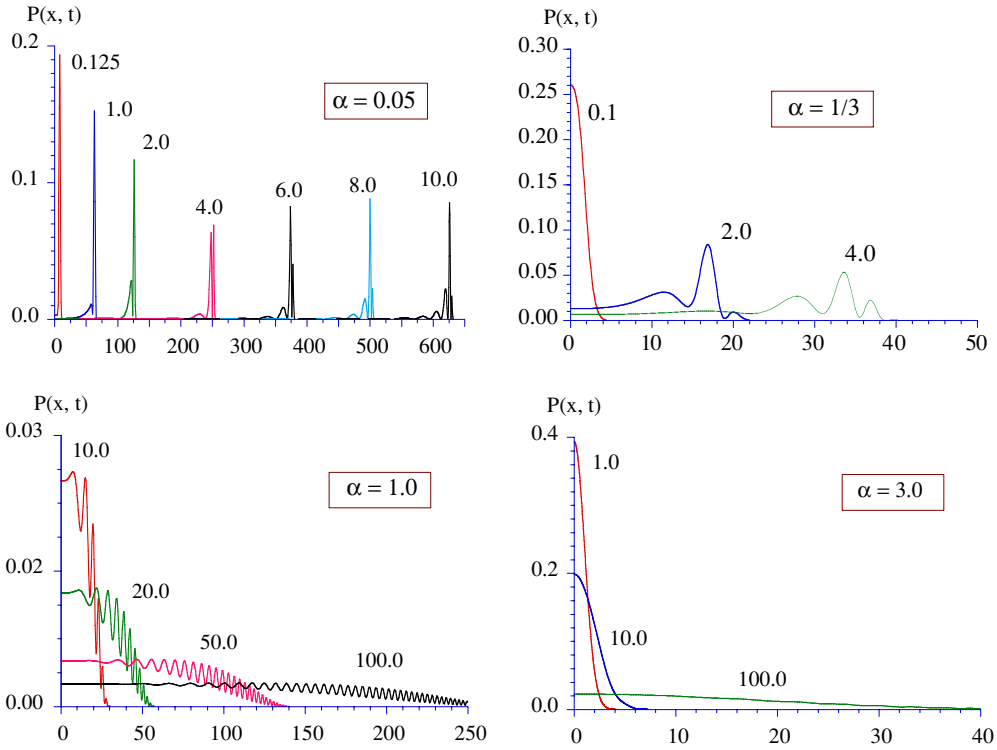

Figure 4. Snapshots of the (symmetric) density profile at successive times t for various values of the parameter α; each curve is labelled by t/T where T is the Larmor period $2\pi/\omega$. The abscissa unit is the width σ of the initial Gaussian packet. Note the different scales from one drawing to another.

parameter α varies. For α small (remember this corresponds to QRW), the (two) peaks structure is clearly visible, and displays small satellites at the back of the packet. They are easily understood as arising from a (quantum) path in which the particle has undergone a small number of precessions, a fact which is confirmed by the $\alpha = 1/3$ curves: it can be checked that the number of peaks at time t is close to t/T, where T is the Larmor period. The extreme-right peak arises when the particle does not precess at all, then comes a secondary peak associated with one precession, and so on. When α increases, the structure is still present but diminishes quickly as time goes on. Eventually, for α large enough, the profile does not display any structure and vaguely looks like a standing Gaussian wave packet. As a whole, the profile is rather sensitive to α; also note that $P(x,t)$ remains notably non-zero in the central region even at large times (see below, especially (5.9)).

Approximate analytical expressions of the density can also be obtained (see appendix). For $\alpha \ll 1$, we find that

$$P(x,t) \simeq \frac{\alpha^2}{16(2\pi)^{3/2}} \left| \int_{-\infty}^{+\infty} \mathrm{d}X' \, \mathrm{e}^{-\frac{1}{4}(X-X'-\frac{vt}{2})^2} H_1^{(2)}(\tilde{X}') \right|^2 \tag{5.7}$$

where $\tilde{X}' = \alpha\sqrt{\frac{vt}{\sigma}|X'|}$ and where $H_1^{(2)}$ is the conventional Hankel function. Details given in the appendix allow us to understand that in this case ($\alpha \ll 1$), the two main peaks moving with the velocity $v/2$ are accompanied by small satellites, corresponding to those quantum paths with a few precessions.

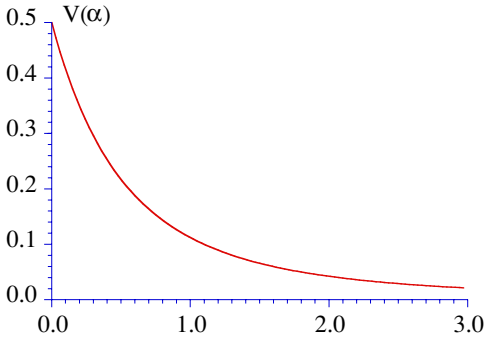

Figure 5. Variation as a function of α of the velocity V of the standard deviation $\Delta x(t)$ (see (5.12)).

On the other hand, for $\alpha \gg 1$, one finds the plain Gaussian distribution:

$$P(x,t) \simeq \frac{1}{\sqrt{2\pi}\,\Delta(t)}\,\mathrm{e}^{-\frac{x^2}{2\Delta(t)^2}}, \qquad \Delta = \sigma\left[1+\left(\frac{v^2 t}{4\sigma^2\omega}\right)^2\right]^{1/2}. \tag{5.8}$$

Because the precession is rapid, the particle does not move in the mean, but the effect is not averaged to zero and produces a linear in time increase of the width of the distribution, as contrasted to the characteristic $\propto t^{1/2}$ Brownian spreading.

Generally speaking, it appears that, for any α, the central region remains populated due to the fact that $P\ (x=0,t)$ decreases rather slowly in time. Indeed, a stationary-phase argument shows that

$$P(x=0,t) \simeq \frac{1}{\sqrt{2\pi}\,\Delta(t)} \sim t^{-1} \qquad \forall t \gg \mathrm{Max}\left(\frac{2\pi}{\omega}, \frac{\sigma}{v}\right). \tag{5.9}$$

As for any initial state, the mean-square dispersion of the coordinate always increases $\propto t$ at large times, and can be readily calculated for the symmetric case, using the results of section 4. In particular, one finds

$$\lim_{t\to+\infty} \frac{\Delta x(t)}{t} = \frac{1}{2}\langle\cos^4\theta\rangle^{1/2} v \equiv V(\alpha)v, \tag{5.10}$$

with

$$\langle\cos^4\theta\rangle = 1+\alpha^2 - \sqrt{2\pi}\,\alpha(3+4\alpha^2)\,\mathrm{e}^{2\alpha^2}[1-\Phi(\sqrt{2}\alpha)], \tag{5.11}$$

where Φ again denotes the probability integral [22]. $V(\alpha)$ is a monotonically decreasing function of α (see figure 5), with the following behaviours:

$$V(\alpha) \simeq \begin{cases} \dfrac{1}{2}\left(1-3\sqrt{\dfrac{\pi}{2}}\alpha^2\right) & \alpha \ll 1 \\ \dfrac{\sqrt{3}}{8\alpha^2} & \alpha \gg 1. \end{cases} \tag{5.12}$$

This means that, apart from small damped in time oscillations, the motion is essentially ballistic, with a velocity $V(\alpha)$ going to zero when the precession frequency increases. With the reduced units used in figure 4, the width of the distribution is $2\pi/(\alpha V(\alpha))(t/T)$; rough estimates show that the gross features of the density profile are in agreement with the latter expression for the standard deviation.

Note that (5.12) says that $V(\alpha)$ goes to $1/2$ in the limit $\alpha = 0+$, a result which is slightly different from that obtained by Konno [23], and rederived by Grimmett *et al* [24], who found

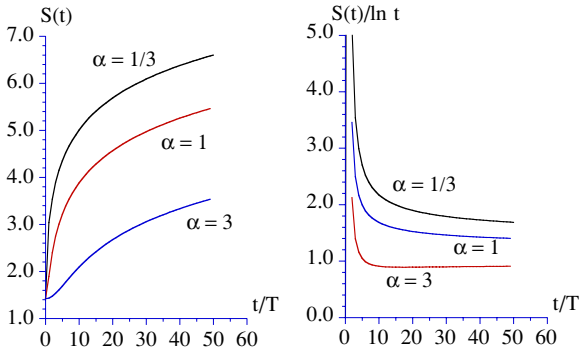

Figure 6. Variation in time of the Shannon entropy $S(t)$ (left). The right part shows the ratio $S(t)/\ln t$, which becomes a constant at large times.

that the velocity tends toward $\sqrt{(2-\sqrt{2})/2} \simeq 0.541\,19$ when the time t goes to infinity. The small numerical discrepancy between the latter result and that expressed by (5.12) can have several origins. First, remember that it is a common fact that discrete versus continuous versions of the same problem differ in numerical details, usually considered as irrelevant, especially when all numbers are of the same order of magnitude. Second, it must be realized that two limits are here involved, namely $\alpha \to 0$ and $t \to \infty$. The lattice version corresponds to the limit $\alpha \to 0$, so that in a discrete framework, the limit $t \to \infty$ is necessarily the last one to be taken. On the opposite, result (5.12) is obtained by looking at the asymptotics $t \to \infty$ in the continuous version and, as a particular case, yields $V(0+) = 1/2$ when alpha goes to zero. In other words, the order of limits is exchanged in the two procedures; no obvious reason guarantees that the two results should coincide, all the more since the limit $\alpha \to 0$ is singular, as emphasized above.

As a final measure of the profile, let us analyse the Shannon entropy, defined as

$$S(t) = -\int_{-\infty}^{+\infty} \mathrm{d}x\, P(x,t) \ln P(x,t). \tag{5.13}$$

Three typical plots are given in the left part of figure 6, showing that $S(t)$—an ever-increasing function in time—changes gently with α and does not display a transition reflecting the bimodal/unimodal cross-over. In addition, it is seen that $S(t) \propto \ln t$ at large times, which means that, as is often the case, $S(t) \propto \ln \Delta x(t)$.

6. Conclusions

In this paper, we presented a simple model describing the dynamics of a particle with a linear dispersion law, when the direction of motion is determined by the value of the spin, the former being able to flip due to magnetic impurity scattering or by coupling with an external field. The resulting intrication between orbital and spin degrees of freedom yields a rather rich and complex dynamics with unexpected features, governed by the single parameter $\alpha = \sigma\omega/v$ measuring the ratio between the time of flight and the Larmor period T.

The most surprising fact is spin-freezing when the width of the initial wave packet becomes quite small: narrowing the latter produces stronger and stronger shielding of the spin which can thus keep for ever the memory of its initial value. This robustness could be of interest in applications where the spin value carries sensitive information, e.g. in spintronics and in quantum spin computation.

Besides this remarkable fact, the density profile itself shows up a variety of shapes which reflect the competition between motion in space and Larmor precession. In the intermediate case where the characteristic time of flight σ/v is of the order of the precession period, the profile displays a rich structure corresponding to the various quantum paths with zero, one, two, ..., precessions: the number of rotations can be directly read by looking at the maxima of the density. In one extreme case ($\alpha \ll 1$), one recovers conventional quantum random walk in a space–time continuous framework, and its characteristic multimodal (bimodal for $J = 1/2$) distribution. In the opposite case $\alpha \gg 1$, the particle hardly moves in the mean because of rapid precession, but the width of the packet increases proportionally to the time t.

Another interesting fact, already discussed in the past in the restricted QRW limit, is the role of the phases present in the initial spin state: it turns out that the spatial probability density is even only when the initial state is an eigenvalue of the transverse spin J_y, i.e. when the coefficients have the same modulus *and* a definite phase relationship. For an infinitely narrow wave packet, this specific property disappears, and the subsequent motion becomes phase independent: we do not have a simple explanation of this phase symmetry breaking.

In all cases, the RMS deviation of the coordinate $\Delta x(t)$ increases like t, much faster than in classical random motion. This universal increase integrates in fact various shapes, from sharp rapidly moving well-defined peaks, to a standing flattening Gaussian distribution. The same can be said about the Shannon entropy, which does not show up any cross-over when α varies; it essentially behaves like $\ln \Delta x$, as is often the case, and thus increases $\propto t$ at times large enough.

Some of our results are restricted to the $J = 1/2$ case. Obviously enough, generalization to arbitrary J is appealing; in particular, it would be interesting to look at the high-J (quasi-classical limit), especially in order to analyse the above-mentioned phase symmetry-breaking phenomenon. Furthermore, it would be interesting to check whether the above shielding effect is robust against phase decoherence, i.e. to develop simple models incorporating coupling to a quantum or classical bath. Work in these directions is in progress.

Acknowledgments

I am indebted to C Caroli, R Mosseri, P Ribeiro and J Vidal for helpful and numerous fruitful discussions.

Appendix

We now briefly sketch the methods allowing us to obtain the approximate expressions (5.7) and (5.8) given in the main text. In all cases, the approximations start with the expression of the time-evolution operator U, and preserve unitarity.

Let us begin with the easiest case, namely $\alpha \gg 1$, i.e. when the spin precesses quickly and when the drift is slow. Then, the angle θ in (3.6) is close to $\frac{\pi}{2}$. From (5.2), one readily obtains

$$\psi_+(x,t) \simeq \frac{1}{(2\pi)^{3/4}\sigma^{1/2}} \int_{-\infty}^{+\infty} \mathrm{d}k\, \mathrm{e}^{-k^2+\mathrm{i}kX}\, \mathrm{e}^{-\mathrm{i}\omega t\sqrt{1+(k/\alpha)^2}/2}, \tag{A.1}$$

and $\psi_-(x,t) = \mathrm{i}\psi_+(-x,t)$. Taking advantage of the Gaussian cut-off, the square-root can be safely expanded when $\frac{k}{\alpha} \sim \frac{1}{\alpha} \ll 1$; the resulting Gaussian integrals are readily evaluated, and one eventually finds the result given in (5.8).

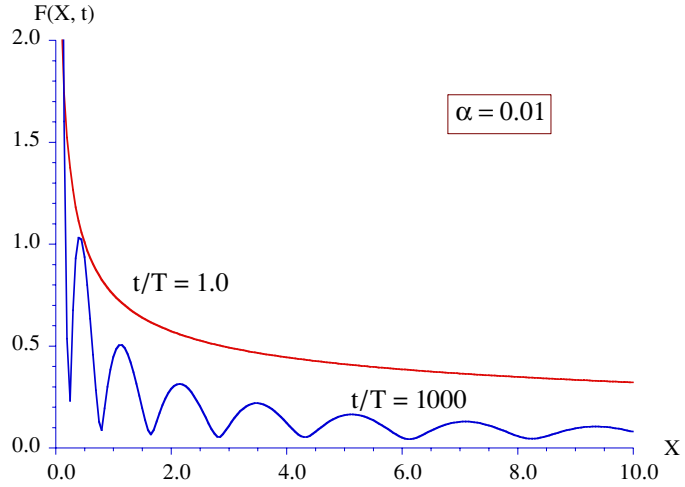

Figure 7. Kernel $F(X,t)$ defined in (A.6) for the convolution (see (A.4)).

The other case, $\alpha \ll 1$, (swift drift and slow precession) is much more involved, due to the fact that the limit $\alpha \to 0$ is highly singular. From (3.6), the expression of ψ_+ is

$$\psi_+(x,t) = \frac{1}{(2\pi)^{3/4}\sigma^{1/2}} \int_{-\infty}^{+\infty} \mathrm{d}k\, \mathrm{e}^{-k^2+\mathrm{i}kX}\, \mathrm{e}^{-\mathrm{i}\frac{vt}{2\sigma}\sqrt{k^2+\alpha^2}}, \tag{A.2}$$

and one still has $|\psi_-(x,t)| = |\psi_+(-x,t)|$. No simple approximation seems possible on such an expression but, since one expects that the rapidly moving peak around $x \sim \frac{vt}{2}$ be slightly modulated by the precession, it is tempting to write an approximation using a convolution integral. For that purpose, we rewrite (A.2) as follows:

$$\psi_+(x,t) = \frac{1}{(2\pi)^{3/4}\sigma^{1/2}} \int_{-\infty}^{+\infty} \mathrm{d}k\, \mathrm{e}^{\mathrm{i}kX}\, \mathrm{e}^{-k^2-\mathrm{i}k\frac{vt}{2\sigma}}\, \mathrm{e}^{\mathrm{i}\frac{vt}{2\sigma}(k-\sqrt{k^2+\alpha^2})}. \tag{A.3}$$

By the convolution theorem, this means that ψ_+ can be expressed as

$$\psi_+(x,t) = \frac{1}{2^{3/4}\pi^{1/4}\sigma^{1/2}} \int_{-\infty}^{+\infty} \mathrm{d}X'\, \mathrm{e}^{-\frac{1}{4}\left(X-X'-\frac{vt}{2\sigma}\right)^2} F(X',t), \tag{A.4}$$

where $F(X,t)$ is the Fourier transform:

$$F(X,t) = \frac{1}{2\pi} \int_{-\infty}^{+\infty} \mathrm{d}k\, \mathrm{e}^{\mathrm{i}kX}\, \mathrm{e}^{\mathrm{i}\frac{vt}{2\sigma}(k-\sqrt{k^2+\alpha^2})}. \tag{A.5}$$

Note that for $\alpha = 0$, $F(X)$ reduces to the Dirac function $\delta(X)$. Now, we expand the (small) phase factor as $k - \sqrt{k^2+\alpha^2} \simeq k - |k|\left(1 + \frac{\alpha^2}{2k^2}\right)$, allowing us to write

$$F(X,t) \simeq f(X,t) - f\left(X + \frac{vt}{2\sigma}, t\right) \tag{A.6}$$

where the function f is defined as

$$f(X,t) = \frac{1}{2\pi} \int_0^{+\infty} \mathrm{d}k\, \mathrm{e}^{\mathrm{i}X[k-\alpha^2 vt/(4\sigma Xk)]}. \tag{A.7}$$

This function can be expressed with the Hankel functions $H_\nu^{(1,2)}(z)$ [22]. A somewhat tedious calculation yields

$$f(X,t) = \frac{\alpha}{4}\,\mathrm{sgn}(X)\sqrt{\frac{vt}{\sigma|X|}}\, H_1^{(2)}\left(\alpha\sqrt{\frac{vt}{\sigma}|X|}\right). \tag{A.8}$$

By (A.6), this completes the determination of the kernel $F(X,t)$; nevertheless, analysis reveals that the second term in (A.6) is quickly negligible, because of the rapid translation of each well-defined peak, so that one nearly always has $F(X,t) \simeq f(X,t)$. Figure 7 shows the variation of $|F(X,t)|$ as a function of the reduced abscissa $X = \frac{x}{\sigma}$, at short and long times. In all cases, the strong peak in $F(X,t)$ near $X = 0$ explains the persistence of the two main peaks in the density $P(x,t)$, whereas slowly decreasing ($\sim X^{-1/2}$) oscillations are responsible for the secondary small peaks located just behind the main one. The minima arise from the zeroes of the Y_1 Bessel function included in $H_1^{(2)}$, which becomes denser and denser as time goes on; this can explain that at large times, the moving peaks for $\alpha \ll 1$ eventually grows up (see figure 4, upper left).

References

[1] Aharonov Y and Davidovich L 1993 Quantum random walks *Phys. Rev.* A **48** 1687
[2] Leggett A J, Chakravarty S, Dorsey A T, Fisher M P A, Garg A and Zwerger W 1987 Dynamics of the disipative two-state system *Rev. Mod. Phys.* **59** 1
[3] Aslangul Cl, Pottier N and Saint-James D 1985 Time-behaviour of the correlation functions in a simple dissipative quantum model *J. Stat. Phys.* **40** 167
[4] Ambainis A, Bach E, Nayak A, Vishwanath A and Watrous J 2001 One-dimensional quantum walks *Proc. 33rd Ann. Symp. on Theory of Computing* (New York: ACM) p 37
[5] Nayak A and Vishwanath Briegel A 2000 Quantum walk on the line *Preprint* quant-ph/0010117
[6] Dür W, Raussendorf R, Kendon V M and Briegel H-J 2002 Quantum random walks in optical lattices *Preprint* quant-ph/0207137
[7] Konno N 2002 Quantum random walks in one dimension *Quantum Inf. Process.* **1** 345 (*Preprint* quant-ph/0206053)
[8] Kempe J 2003 Quantum random walks—an introductory overview *Preprint* quant-ph/0303081
[9] Gardiner C W 1990 *Handbook of Stochastic Methods* (Berlin: Springer)
[10] Blanchard Ph and Hongler M-O 2004 Quantum random walks and piecewise deterministic evolutions *Phys. Rev. Lett.* **92** 120601
[11] Misra B and Sudarshan E C G 1977 The Zeno's paradox in quantum theory *J. Math. Phys.* **18** 756
[12] Itano W M, Heinzen D H, Bolllinger J J and Wineland D J 1990 Quantum Zeno effect *Phys. Rev.* A **41** 2295
[13] Kempe J 2002 Quantum random walk hits exponentially faster *Preprint* quant-ph/0205083
[14] Luttinger J M 1963 An exactly soluble model of a many-fermion system *J. Math. Phys.* **9** 1154
[15] Vagner I D 2004 Nuclear spintronics: quantum Hall and nano-objects *Preprint* cond-mat/0403087
[16] McGuire J P, Ciuti C and Sham L J 2004 Theory of spin transport induced by ferromanetic proximity on a two-dimensional electron gas *Phys. Rev.* B **69** 115339
[17] Yang C-K, Zhao J and Lu J P 2003 Magnetism of transition-metal/carbon-nanotube hybrid structures *Phys. Rev. Lett.* **90** 257203
[18] Levitov L S and Rashba E I 2004 Dynamical spin-electric coupling in a quantum dot *Phys. Rev.* B **69** 115324
[19] Dyakonov M I 2004 Spintronics? *Preprint* cond-mat/0401369
[20] de Gennes P G 1966 *Superconductivity of Metals and Alloys* (New York: Benjamin)
[21] Takayama H, Lin-Liu Y R and Maki K 1980 Continuum model for solitons in polyacetylene *Phys. Rev.* B **21** 2388
[22] Gradshteyn I S and Ryzhik I M 1980 *Table of Integrals, Series and Products* (New York: Academic)
[23] Konno N 2002 A new type of limit theorems for the one-dimensional quantum random walk *Preprint* quant-ph/0206103
[24] Grimmett G, Janson S and Scudo P F 2003 Weak limits for quantum random walks *Preprint* quant-ph/0309135